Flow Field Upstream of an Orifice under Fixed Bed and Equilibrium Scour Conditions

D. N. Powell, A.M.ASCE[1]; and A. A. Khan, F.ASCE[2]

Abstract: Flow behavior upstream of a circular orifice with the invert at the bed level (initially) is investigated under fixed bed and equilibrium scour (mobile bed) conditions. The experiments are performed under three different constant heads and sediment sizes. Longitudinal and vertical components of velocity are measured in the vertical and horizontal planes passing through the center of the orifice. The velocity decay upstream of the orifice (along the centerline of the orifice) is slower for the fixed bed case than for the unbounded orifice. Under equilibrium scour condition, the velocity decay transitions from the velocity profile for the unbounded orifice to the fixed bed condition. The longitudinal velocity profiles in the horizontal plane at different locations upstream of the orifice are found to be similar for both fixed and mobile bed cases. The longitudinal velocity profiles in the vertical plane are also found to be similar for each case. The maximum velocity is found to occur below the centerline of the orifice for both cases. The location and decay of maximum velocity with distance upstream of the orifice are quantified. A three-dimensional flow model is used to simulate the flow behavior upstream of the orifice under fixed bed and equilibrium scour conditions. The model accurately predicts the velocity field upstream of the orifice under both fixed bed and mobile bed conditions. **DOI: 10.1061/(ASCE)HY.1943-7900.0000960.**

Author keywords: Circular orifice; Flow behavior; Fixed bed; Equilibrium scour; Computational modeling.

Introduction

Orifices are common appurtenances in hydraulic structures. Orifices near the base of dams may be used for hydropower generation, flow control, and/or sediment removal. Fish entrainment during hydropower generation is another major concern because it depends on velocity magnitude and acceleration field near the orifice (Coutant and Whitney 2000). Thus, studying the flow field upstream of orifices is of interest under variety of situations.

Flow upstream of an unbounded circular orifice is well understood (Anayiotos et al. 1995; Shammaa et al. 2005; Bryant et al. 2008). Islam and Zhu (2011) investigated flow behavior upstream of two-dimensional intakes situated near a fixed bed. Chanson et al. (2002) studied the unsteady flow behavior upstream of an unbounded orifice under a falling head test. Understanding flow upstream of orifices is critical for turbine intake and fish entrainment. For example, Bhuiyan et al. (2009) simulated flow upstream of a dam to study the risk of fish entrainment into the intakes. Khan et al. (2004) simulated flow upstream of a turbine intake to study the impact of flow blockage attributable to trash collection at rakes. Powell and Khan (2011, 2012) investigated sediment transport mechanism and the resulting equilibrium scour hole profile upstream of a circular orifice. Prohaska et al. (2010a, b) investigated the outflow characteristics of circular orifices in riser pipes. A jet flowing out of an opening over a movable bed was studied by Kurniawan et al. (2004) and Rajaratnam and Berry (1977). They observed that the location of the maximum velocity began at the jet centerline and dropped below the centerline further downstream in the scour hole. Next, the maximum velocity moved upward at the extremity of the scoured area.

The aim of this paper is to report results of the flow field upstream of an orifice under fixed bed and equilibrium scour (mobile bed) conditions, which has not been reported before. The data from physical model study are used to verify the simulation capability of a three-dimensional computational model under fixed bed and equilibrium scour conditions.

Experimental Setup

The experiments were conducted in a rectangular box 3.5 m long (x-direction), 2.13 m wide (y-direction), and 1.22 m deep (z-direction). The origin of the coordinates system, located at the invert of the orifice, and the cross-sectional view of the experimental setup, are shown in Fig. 1. The first 1.07-m length of the box was used as flow inlet and mesh placement for flow distribution and straightening, leaving a clear length of 2.44 m upstream of the orifice. A circular orifice, 15.24 cm in diameter (d), was located at midwidth. The invert of the orifice was 22.86 cm above the bed. For fixed bed tests, a false floor was placed at the invert level of the orifice. For the mobile bed cases, the 22.86-cm space between the invert of the orifice and the floor of the tank was filled with sediment. In all cases, the invert of the orifice was initially set at the bed level. Further details regarding experiment setup are given by Powell and Khan (2012).

For the mobile bed case, three different noncohesive sediment sizes were used, labeled as fine (F), medium (M), and coarse (C). The median sizes of the sand were 0.29, 0.73, and 0.89 mm, respectively. The gradation coefficients, as defined by Wu (2008), for the fine, medium, and coarse sand were 1.5, 1.46, and 1.31, respectively. Fixed bed and mobile bed tests were run under three different constant heads (above the center of orifice). The details about these tests are given in Table 1. In the case of mobile bed tests, the tests were run until equilibrium scour was achieved.

[1]Former Graduate Student, 110 Lowry Hall, Glenn Dept. of Civil Engineering, Clemson Univ., Clemson, SC 29634-0911.

[2]Associate Professor, 218 Lowry Hall, Glenn Dept. of Civil Engineering, Clemson Univ., Clemson, SC 29634-0911 (corresponding author). E-mail: abdkhan@clemson.edu

Note. This manuscript was submitted on January 30, 2014; approved on October 2, 2014; published online on November 6, 2014. Discussion period open until April 6, 2015; separate discussions must be submitted for individual papers. This paper is part of the ***Journal of Hydraulic Engineering***, © ASCE, ISSN 0733-9429/04014076(8)/$25.00.

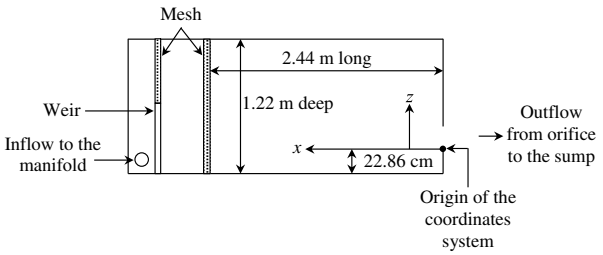

Fig. 1. Vertical profile of the experimental setup

The equilibrium scour condition was assumed when the bed profile upstream of the orifice at $y = 0$ did not change more than 2 mm in 24 h. The test duration lasted up to three days. The velocity data were collected once the equilibrium scour was reached, as described by Adduce and Sciortino (2006) and Adduce and La Rocca (2006).

The x, y, and z components of the velocity (u, v, and w, respectively) were measured with a Sontek (San Diego) 16-MHz acoustic Doppler velocimeter (ADV). The ADV can measure velocity up to 250 cm/s with accuracy of 0.1%. The velocity at each point was measured for 90 s at a rate of 50 Hz and averaged. The average velocity through the orifice (U_o), defined as volumetric flow rate per unit orifice area, was 1.846 to 2.473 m/s under the fixed bed and mobile bed conditions for three different heads.

Numerical Model

A three-dimensional flow model called *Flow-3D* was used to simulate flow pattern upstream of the orifice under fixed bed and equilibrium scour conditions. The model uses three-dimensional Reynolds-averaged Navier-Stokes equations. In this study, the $k-\varepsilon$ turbulence closure scheme with standard coefficients was used. Complete details about the model are given by Aziz et al. (2008), Aziz and Khan (2011), and Raiford and Khan (2013). The actual physical model dimensions for width and depth were used in simulations, whereas only the clear length of 2.44 m after the mesh was used in the simulation. In the physical model, the orifice was cut in 6-mm-thick Plexiglas, the same wall thickness for the orifice was used in the simulation to ensure that jet contraction and flow behavior were exactly replicated. The measured bed topography at equilibrium scour condition was used in the simulation for the mobile bed cases. A rectangular, nonuniform grid was used. For $x < 2d$, mesh size was set to a 1.9-cm^3, and the mesh size was 3.8-cm^3 outside this region. To ensure mesh-independent solutions, a finer mesh of 0.89-cm^3 was used within the $x < 2d$ region and a 1.9-cm^3 was used elsewhere. The maximum velocity difference as a result of mesh refinement occurred in the longitudinal velocity component along the centerline of the orifice. The difference in the longitudinal velocity decay with distance along the centerline of the orifice based on the two meshes was less than 1%. In addition, the velocity profiles did not change in the vertical and horizontal planes within the high acceleration zone ($x < 2d$). The numerical results shown in this paper were obtained using the coarser mesh.

For the mobile bed cases, the surface roughness was assumed as the median size of the sediment. In the case of fixed bed simulation, the surface roughness of 0.05 mm was used. During simulation, the inflow boundary with specified discharge was established at the upstream end of the tank and a nonreflective boundary condition (where the normal derivatives are assumed to be zero) was established at the outlet boundary. Two different scenarios were modeled for the location of the outflow boundary. In the first case, the domain terminated at the orifice and the outlet boundary condition was applied at the orifice. In the second case, the computational domain was extended by 1 m beyond the orifice to include the free jet issuing from the orifice, and the outlet boundary condition was applied at the end of the extended domain. The two cases provided the same results for the flow filed upstream of the orifice. The water level in the tank was established per test specification in the physical model. In the model, the free surfaces of the free jet issuing from the orifice were tracked by using the modified volume of fluid (VOF) method.

Table 1. Description of Experimental Tests

Test	Head (cm)	Bed type	Test	Head (cm)	Bed type
H1	45.72	Fixed	H1M	45.72	Medium
H2	60.96	Fixed	H2M	60.96	Medium
H3	76.20	Fixed	H3M	76.20	Medium
H1F	45.72	Fine	H1C	45.72	Coarse
H2F	60.96	Fine	H2C	60.96	Coarse
H3F	76.20	Fine	H3C	76.20	Coarse

Results

Variation of Longitudinal Velocity along the Centerline of the Orifice

The variation of longitudinal velocity along the centerline of the orifice (u_c) is investigated (i.e., $y = 0$ and $z = 0.5d$). For the unbounded orifice, the longitudinal velocity along the centerline of the orifice, based on the potential flow theory (Shammaa et al. 2005; Bryant et al. 2008), is given by Eq. (1), where $a_1 = 0.25$, $b_1 = 2$, $c_1 = 0.5$, $x_o = x/d$, and U_o = average velocity through the orifice

$$\frac{u_c}{U_o} = 1 - \left(1 + \frac{a_1}{x_o^{b_1}}\right)^{-c_1} \tag{1}$$

The longitudinal velocity profiles along the centerline of the orifice for the fixed bed (three tests) and mobile bed (none tests) cases were plotted and fitted with Eq. (1) because it satisfies the limit conditions. The a_1, b_1, and c_1 values are 0.332, 1.679, and 0.515, and 0.145, 1.493, and 0.913 for the fixed bed and mobile bed cases, respectively. The coefficient of determination (R^2) is 0.99 for both fits. The longitudinal velocity decay along the centerline of the orifice for the three cases is shown in Fig. 2. In the case of the fixed bed, the velocity is higher than that of the unbounded orifice owing to the proximity of the solid boundary, which limits the area through which the fluid is withdrawn. For the mobile bed, the velocity is lower than that for the case of the unbounded orifice for $x_o \leq 1$; outside this region, the velocity approaches that of the fixed bed case. At the end of the scour hole, the velocities for the fixed bed and mobile beds merge and are higher than the velocity resulting from an unbounded orifice. The length of the scour hole ranges from $1.5d$ to $2.17d$. The length of the scour hole increases with the head over the orifice and has a decreasing tendency with the increase in sediment size. It can be concluded that the velocity in the case of the mobile bed approaches that for the fixed bed case at the end of the scour hole.

The comparison between numerical results and measured data for longitudinal velocity decay along the centerline of the orifice for the fixed bed (H1) and mobile bed (H1F) cases are shown in Fig. 3. For clarity, the measured data and simulated results for the mobile

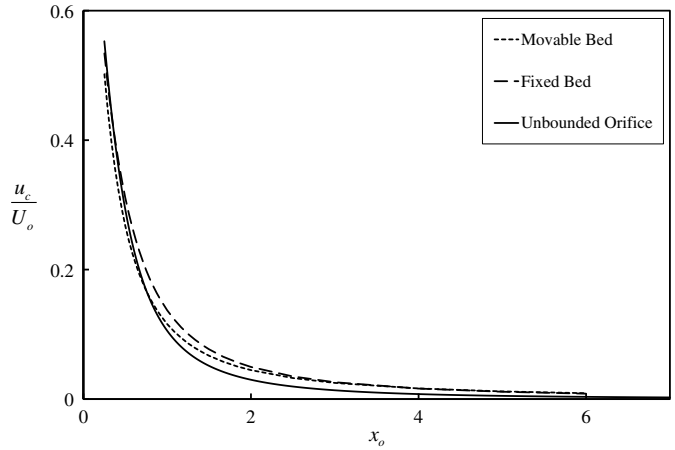

Fig. 2. Decay of the longitudinal velocity along the center of the orifice

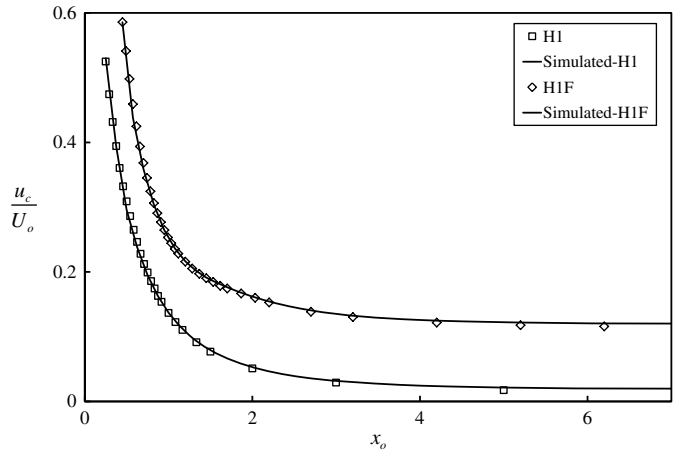

Fig. 3. Comparison of numerical and measured longitudinal velocity along the centerline of the orifice for fixed and mobile beds (mobile bed results are offset by 0.1 and 0.2 along x-axis and y-axis, respectively)

bed are offset by 0.2 and 0.1 for x_o and u_c/U_o, respectively. The model accurately predicts the decay of the longitudinal component of the velocity along the centerline of the orifice. The simulated results for other heads and sediment sizes show similar trend.

Longitudinal Velocity Profiles in Horizontal Plane

The longitudinal velocity profiles at different locations in a horizontal plane ($x - y$ plane) passing through the center of the orifice were measured. The velocity profiles are nondimensionalized by using the maximum velocity (u_{my}) within the corresponding profile as the velocity scale and b_y as length scale, similar to the study of circular wall jets by Wu and Rajaratnam (1990). The length scale, b_y, represents the lateral distance between the maximum velocity and the point where $u = 0.5u_{my}$. The velocity profiles in the horizontal plane passing through the center of the orifice are symmetrical and the maximum velocity occurs at $y = 0$, i.e., $u_{my} = u_c$. The nondimensional velocity profiles in the horizontal plane for the fixed bed and mobile bed are fitted by using Eq. (2), where $y_n = y/b_y$. The fit parameters for the fixed bed and mobile bed cases are $a_2 = 0.6773$, $b_2 = 1.821$, and $a_2 = 0.6573$, $b_2 = 1.756$, respectively. The coefficient of determination in both cases

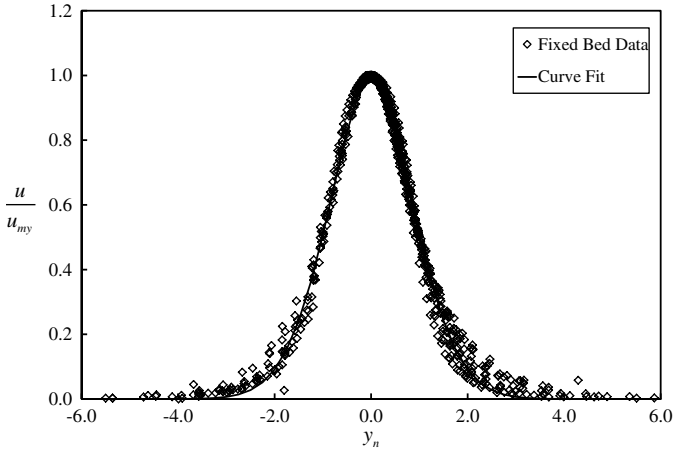

Fig. 4. Nondimensional velocity profiles in horizontal plane for fixed bed

is 0.99. The difference between the two fitted curves is very small (maximum difference of 0.0029), thus either curve can be used for both cases:

$$\frac{u}{u_{my}} = \exp(-a_2|y_n|^{b_2}) \tag{2}$$

The nondimensional velocity profiles along with the fitted curves, for the fixed bed and mobile bed cases, are shown in Figs. 4 and 5, respectively. Data for all heads and sediments sizes are shown in these figures. Outside the region of $y_n = \pm 1.5$, the measured data for velocity profiles show scatter. The scatter is more pronounced at outer edges in the case of the mobile bed. In addition, the scatter at the outer edges does not show any trend with the head or sediment size. The variation in length scale, b_y, for both cases is shown in Fig. 6. The slope and intercept values for the fixed bed and mobile bed cases are 0.637, 0.3428 and 0.732, 0.2921, respectively. The results show that the velocity profiles spread out more for the mobile bed case.

Longitudinal Velocity Profiles in Vertical Plane

The longitudinal velocity profiles at different locations in a vertical plane ($x - z$ plane) passing through the center of the orifice are measured for the fixed bed and mobile bed cases. The maximum

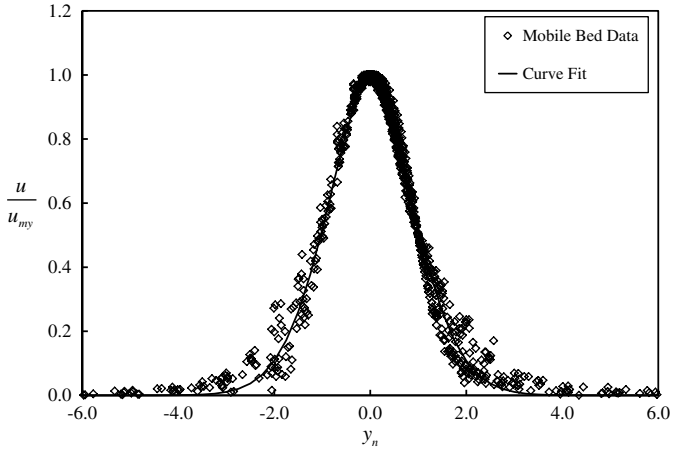

Fig. 5. Nondimensional velocity profiles in horizontal plane for mobile bed

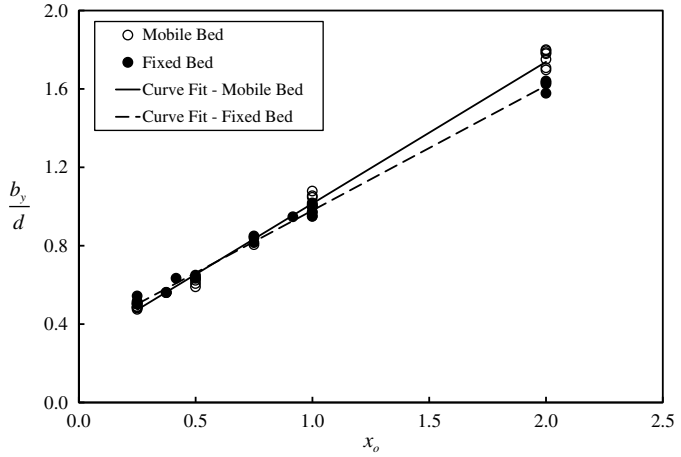

Fig. 6. Variation of lateral length scale

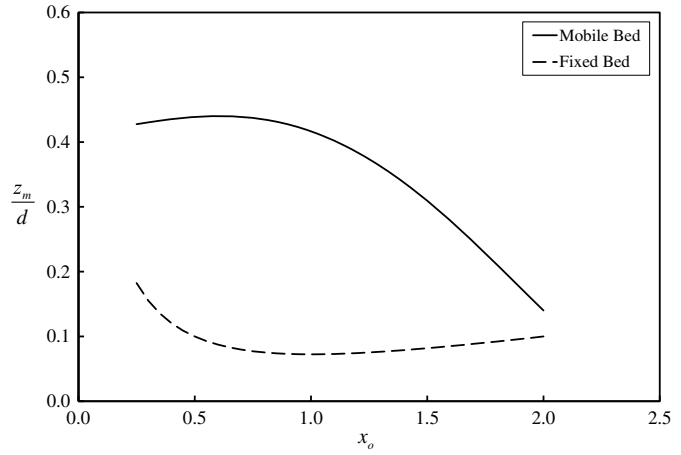

Fig. 7. Variation of the location of maximum velocity with distance upstream of the orifice

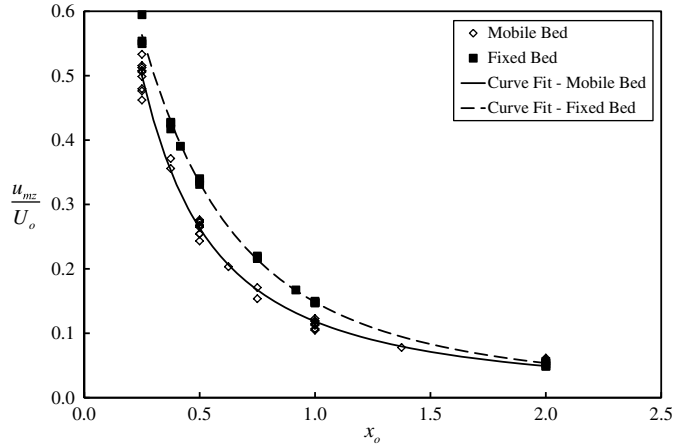

Fig. 8. Variation of maximum velocity with distance upstream of the orifice

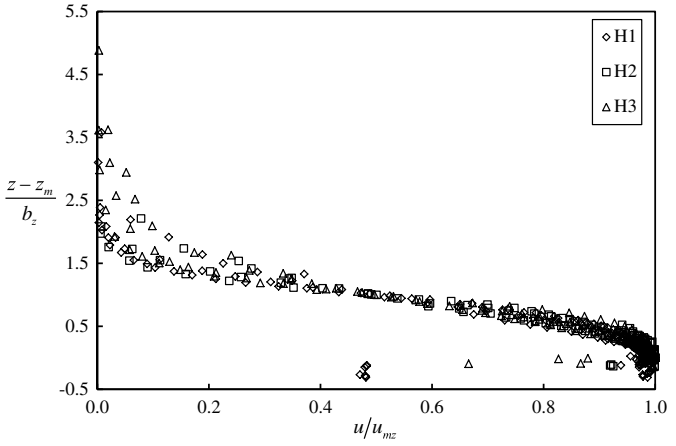

Fig. 9. Nondimensional velocity profiles in vertical plane for fixed bed

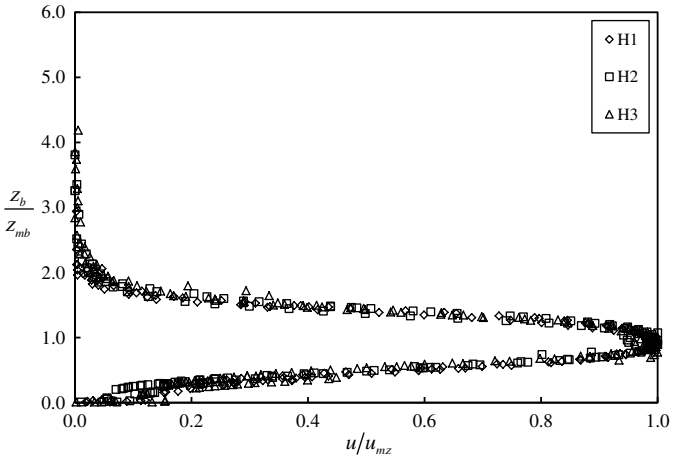

Fig. 10. Nondimensional velocity profiles in vertical plane for mobile bed at $x_o = 0.25$

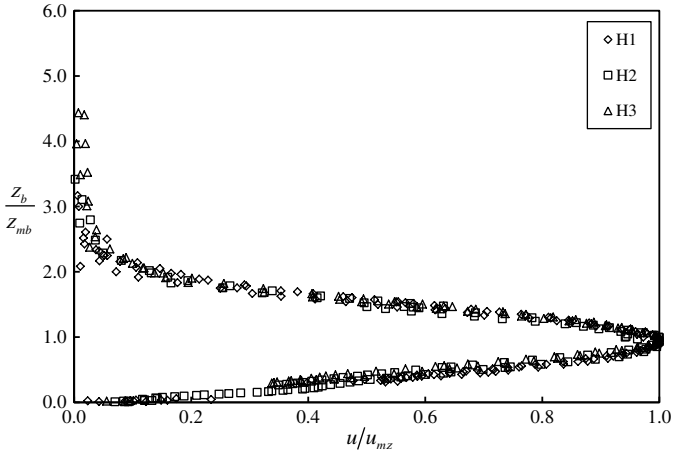

Fig. 11. Nondimensional velocity profiles in vertical plane for mobile bed at $x_o = 0.50$

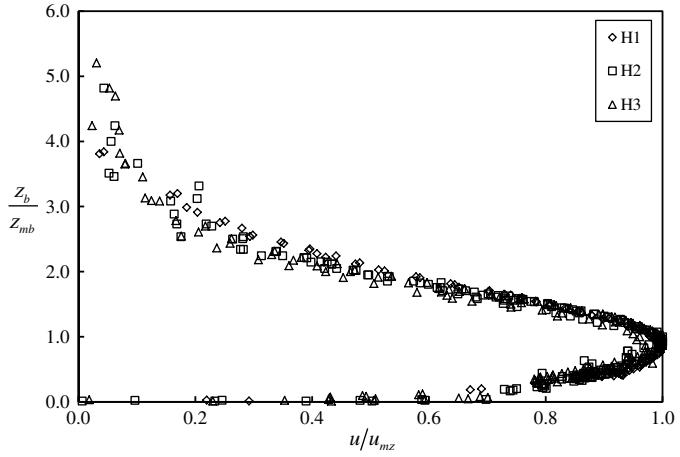

Fig. 12. Nondimensional velocity profiles in vertical plane for mobile bed at $x_o = 1.00$

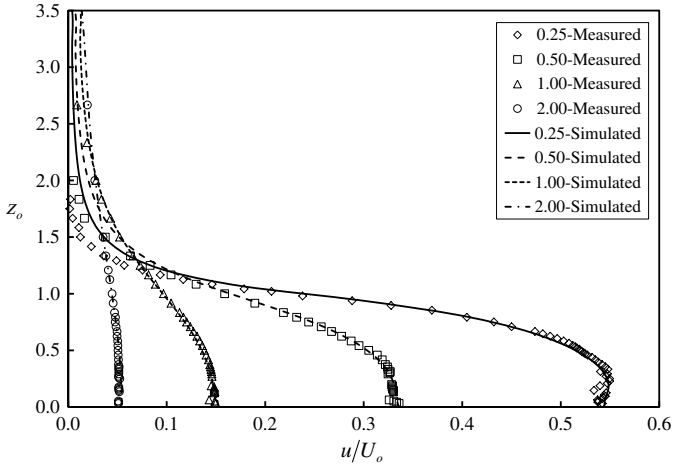

Fig. 14. Comparison of simulated and measured velocity profiles at different x_o in the $x - z$ plane at $y = 0$ for the fixed bed case (H1)

velocity for the unbounded orifice occurs along the center of the orifice. The maximum velocity (u_{mz}) for the fixed bed and mobile bed cases occurs below the center of the orifice and its location changes with the distance upstream. The variations in location, z_m, of the maximum velocity measured from the invert of the orifice with distance upstream of the orifice for the fixed bed and mobile bed cases are shown in Fig. 7. In the figure, only the fitted curves as given by Powell and Khan (2012) are shown. The location of the maximum velocity moves toward the bed in both cases. In the case of movable bed, the location of the maximum velocity approaches that of the fixed bed case at the end of the scour hole. The variations in maximum velocity with the distance upstream of the orifice for the fixed bed and mobile bed cases are shown in Fig. 8. Curves of the form given by Eq. (1) are fitted to the data in each case, and the parameters a_1, b_1, and c_1 have values of 0.338, 1.686, and 0.551, and 0.0786, 1.358, and 1.665 for the fixed bed and mobile bed cases, respectively. Similar to the velocity decay along the centerline of the orifice, the maximum velocity for the mobile bed case is lower than that for the fixed bed case and approaches it at the end of the scour hole.

The longitudinal velocity profiles in the vertical plane for the fixed bed case are nondimensionalized by using the maximum velocity (u_{mz}) within the corresponding profile as velocity scale, and the distance above the maximum velocity to the point where $u = 0.5u_{mz}$, denoted by b_z, as length scale. In addition, the z-coordinate origin is shifted to the location of the maximum velocity. The results are shown in Fig. 9. The velocity profile shows some spread near the outer edge. In addition, the velocity profiles below the maximum velocity do not exhibit similarity. These results are similar to that found for the circular wall jets by Wu and Rajaratnam (1990) and for the circular jets in shallow waters by Raiford and Khan (2009).

For the mobile bed case, similarity between velocity profiles in the vertical plane at different locations upstream of the orifice could

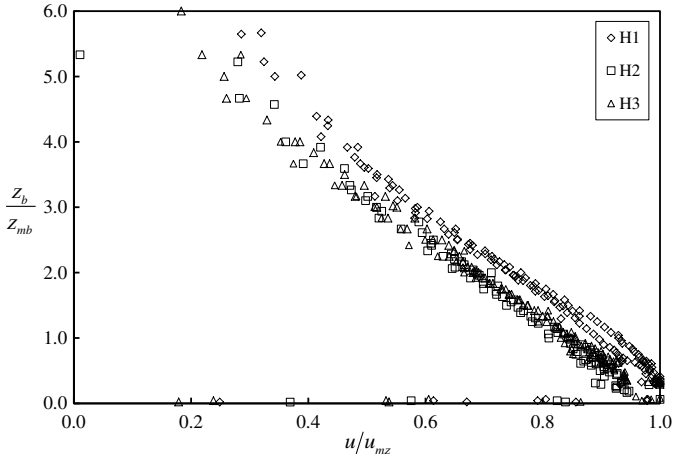

Fig. 13. Nondimensional velocity profiles in vertical plane for mobile bed at $x_o = 2.00$

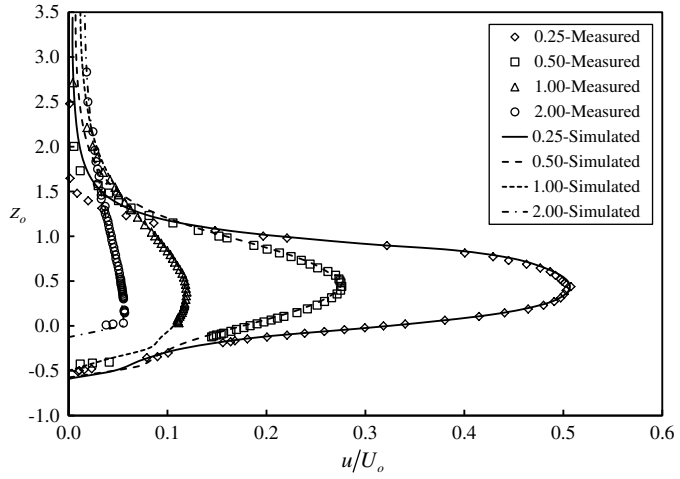

Fig. 15. Comparison of simulated and measured velocity profiles at different x_o in the $x-z$ plane at $y=0$ for the mobile bed case (H1F)

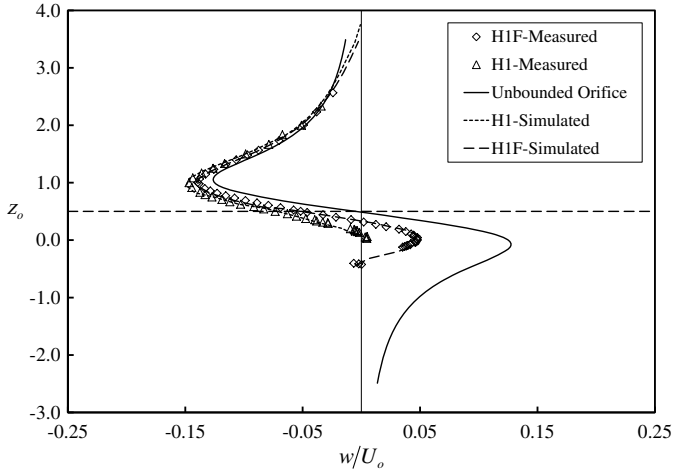

Fig. 17. Vertical velocity profiles in the vertical plane at $x_o=0.5$

not be achieved. However, by using maximum velocity (u_{mz}) as the velocity scale and the height above the scoured bed level to the location of the maximum velocity (z_{mb}) as the length scale, the velocity profiles at a given distance upstream of the orifice are found to be similar for different heads and sediment sizes. The vertical distance is measured from the scoured bed and is denoted by z_b, i.e., $z_b = z - z_s$, where z_s is the scour depth under equilibrium scour condition (negative for vertical distance measured below the origin). The results at different locations upstream of the orifice are shown in Figs. 10–13. The velocity profiles are similar for different heads and sediment sizes at $0.25d, 0.5d$, and $1.0d$. At $2.0d$, the velocity profiles for the smallest head (H1) are not similar to the velocity profiles for the other heads. This is because for the lowest heads, the length of the scour hole is the smallest and less than $2.0d$. Thus, the velocity profiles for the smallest head are outside the scour hole and are not similar to the profiles at higher heads, which are within the scour hole.

The length scales for the fixed bed (b_z) and mobile bed (z_{mb}) are nondimensionalized with orifice diameter and plotted against x_o, a procedure adopted earlier for analyzing the length scale, b_y. Both scales vary linearly with distance. The slope and intercept values for b_z and z_{mb} are 0.58, 0.612 ($R^2 = 0.99$) and 0.333, 1.183 ($R^2 = 0.94$), respectively.

The numerical results for the longitudinal velocity profiles in the vertical plane at different x_o values are compared with the measured data for the fixed bed and mobile bed cases in Figs. 14 and 15, respectively, where $z_o = z/d$. The model accurately predicts the velocity profiles at various locations upstream of the orifice both for fixed bed and mobile bed conditions. The results for other heads and sediment sizes are similar to the results presented here. In the case of the fixed bed, the accelerating flow suppresses the boundary layer development. The closest measurement point to the bed was 0.18 cm away from the bed; at this point, the velocity is close to the maximum value. Thus, the boundary layer thickness based on the measured data is less than 2 mm. The simulated results for the fixed bed show the same trend. The coarse mesh had the closest velocity point 0.15 cm away from the bed; for the fine mesh, the closest point was 0.08 cm away from the bed (the velocity is calculated at the center of the cell). The data point at the bed that will have zero velocity is not plotted because it will assume a linear profile for the boundary layer. In the case of the mobile bed, the scour hole allows the orifice to behave more like an unbounded orifice and the velocity profiles below the center of the orifice have two distinct regions: the upper region close to the orifice is attributable to the unbounded nature of the orifice and the sudden change in the lower part reflects the influence of the bed.

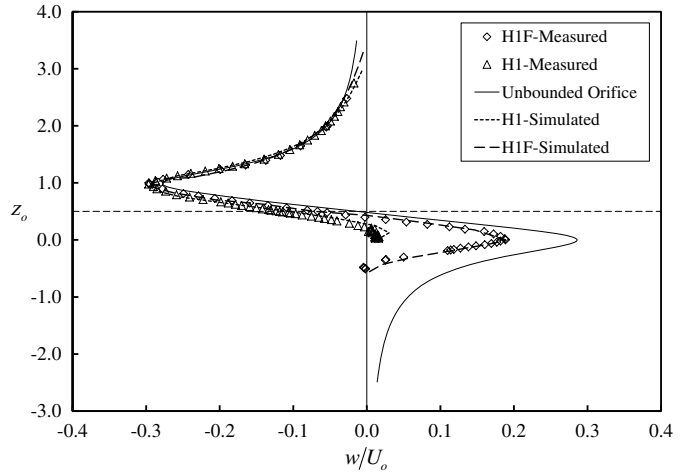

Fig. 16. Vertical velocity profiles in the vertical plane at $x_o=0.25$

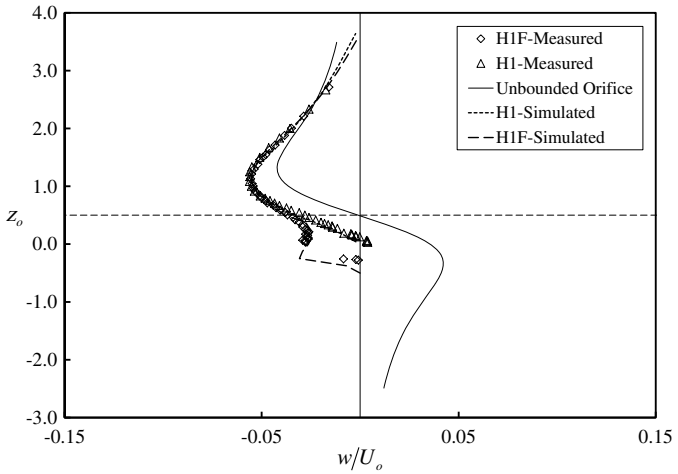

Fig. 18. Vertical velocity profiles in the vertical plane at $x_o=1.0$

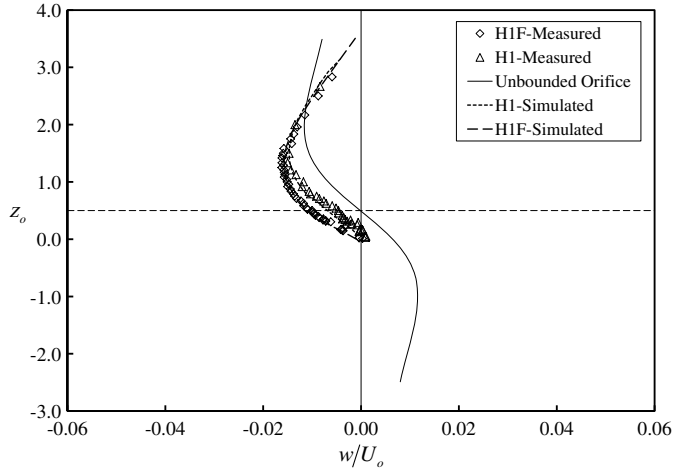

Fig. 19. Vertical velocity profiles in the vertical plane at $x_o = 2.0$

Vertical Velocity Profiles in the Vertical Plane

The vertical velocity profiles (measured and simulated) in a vertical plane ($x - z$ plane) passing through the center of the orifice at different locations upstream of the orifice are shown in Figs. 16–19. The horizontal lines in the figures show the centerline of the orifice. The velocity profiles above the center of the orifice for the fixed bed and mobile bed cases are similar. However, owing to the presence of scour holes, the velocity profiles below the center of the orifice are different. At the end of the scour hole ($x_o = 2.0$), the velocity profiles below the center of the orifice for the two cases follow the same trend. The simulated results for the velocity profile compare well with the measured data.

Conclusions

Flow behavior upstream of a circular orifice is investigated under fixed bed and equilibrium scour conditions. Three different sediment sizes are used. Three different heads over the orifice are used for the fixed bed case and for each sediment size in the mobile bed case. The proximity of the bed restricts the area through which the fluid can be withdrawn and changes the flow behavior upstream of the orifice. The maximum longitudinal velocity at any location upstream of the orifice for the fixed bed and mobile bed cases occurs below the center of the orifice, whereas it occurs along the centerline of the orifice for the unbounded orifice. By choosing suitable length and velocity scales, the longitudinal velocity profiles in the horizontal plane passing through the center of the orifice at different locations upstream of the orifice are similar for both fixed bed and mobile bed cases. The variation of length scale with distance upstream of the orifice is found to be linear for both cases, with velocity profile for the mobile bed case spreading faster than the fixed bed case.

The longitudinal velocity profiles at different locations in the vertical plane passing through the center of the orifice are similar for the fixed bed case. However, the similarity is only restricted to the velocity profile above the maximum velocity. In the case of the mobile bed, the velocity profile at a given location for different heads and sediment sizes are similar. The length scales used to achieve similarity have linear variation with distance upstream of the orifice.

The longitudinal velocity decay upstream of the orifice along the centerline of the orifice is investigated. For the fixed bed case, the velocity is higher than that for the unbounded orifice. In the case of the mobile bed, the velocity close to the orifice is lower than that of the unbounded orifice, and away from the orifice, the velocity approaches that of the fixed bed case. The variation in the maximum longitudinal velocity that occurs below the centerline of the orifice follows the same trend as that of the variation in longitudinal velocity along the centerline of the orifice.

The variation of the vertical component of velocity in the vertical plane passing the center of the orifice is also considered. The vertical velocity above the center of the orifice at different locations for the fixed bed and mobile bed cases are similar. However, below the center of the orifice, the presence of the scour hole significantly impacts the vertical velocity.

A numerical model with the standard $k - \varepsilon$ turbulence closure scheme is used to simulate the fixed bed and mobile bed cases. The simulated velocity profiles in the vertical plane are compared with the measured data. The model is capable of accurately simulating velocity profiles for the flat bed case and within the scour hole for the mobile bed case. In addition, the decay of velocity along the centerline of the orifice and location and magnitude of longitudinal maximum velocity are accurately predicted. The study shows that a numerical model can provide satisfactory results in simulating the flow field upstream of the orifice for the fixed bed and mobile bed cases. Thus, computational models can be used to study flow patterns near outlets of different geometry and configuration (such as multiple outlets in various configurations), which may be important for fish migration studies.

Acknowledgments

The authors would like to acknowledge Ms. Nighat Yasmin's help in producing the appropriate CAD files and accurate conversion to stereolithographic (stl) file needed for simulating the flow upstream of the orifice.

Notation

The following symbols are used in this paper:

b_y = length scale for velocity profiles in the horizontal plane (m);
b_z = length scale for velocity profiles in the vertical plane (m);
d = diameter of orifice (m);
U_o = velocity at the orifice (m/s);
u_c = velocity along the centerline of the orifice (m/s);
u_{my} = maximum velocity for profiles in the horizontal plane (m/s);
u_{mz} = maximum velocity for profiles in the vertical plane (m/s);
u, v, w = velocities in x, y, z directions (m/s);
x_o = nondimensional distance upstream of orifice;
x, y, z = Cartesian coordinates (m);
y_n = nondimensional lateral coordinate;
z_b = vertical distance measured from bed (m);
z_m = location of maximum velocity from origin (m);
z_{mb} = location of maximum velocity from bed (m); and
z_o = nondimensional vertical coordinate.

References

Adduce, C., and La Rocca, M. (2006). "Local scouring due to turbulent water jets downstream of a trapezoidal drop: Laboratory experiments and stability analysis." *Water Resour. Res.*, 42(2).

J. Hydraul. Eng.

Adduce, C., and Sciortino, G. (2006). "Scour due to a horizontal turbulent jet: Numerical and experimental investigation." *J. Hydraul. Res.*, 44(5), 663–673.

Anayiotos, A. S., Perry, G. J., Myers, J. G., Green, D. W., Fan, P. O., and Nanda, N. C. (1995). "A numerical and experimental investigation of the flow acceleration region proximal to an orifice." *Ultrasound Med. Biol.*, 21(4), 501–516.

Aziz, T. N., and Khan, A. A. (2011). "Simulation of vertical plane turbulent jet in shallow water." *Adv. Civ. Eng.*, 2011, 1–10.

Aziz, T. N., Raiford, J. P., and Khan, A. A. (2008). "Numerical simulation of turbulent jets." *Eng. Appl. Comput. Fluid Mech.*, 2(2), 234–243.

Bhuiyan, F., Zhu, D. Z., Leake, A., and Higgins, P. (2009). "Computational fluid dynamics modeling of flow pattern induced by hydropower intakes for fish entrainment assessments." *Proc., 33th Int. Association of Hydraulic Engineering and Research (IAHR)*, Madrid, Spain.

Bryant, D. B., Khan, A. A., and Nadim, N. M. (2008). "Flow field upstream of an orifice." *J. Hydraul. Eng.*, 10.1061/(ASCE)0733-9429(2008)134:1(98), 98–104.

Chanson, H., Aoki, S. I., and Maruyama, M. (2002). "Unsteady two-dimensional orifice flow: A large size experimental investigation." *J. Hydraul. Res.*, 40(1), 63–71.

Coutant, C. C., and Whitney, R. R. (2000). "Fish behavior in relation to passage through hydropower turbines: A review." *Trans. Am. Fish. Soc.*, 129(2), 351–380.

Flow-3D [Computer software]. Santa Fe, NM, Flow Science.

Islam, M., and Zhu, D. (2011). "Flow upstream of two-dimensional intakes." *J. Hydraul. Eng.*, 10.1061/(ASCE)HY.1943-7900.0000284, 129–134.

Khan, L. A., Wicklein, E. A., Rashid, M., Ebner, L. L., and Richards, N. A. (2004). "Computational fluid dynamics modeling of turbine intake hydraulics at a hydropower plant." *J. Hydraul. Res.*, 42(1), 61–69.

Kurniawan, A., Altinakar, M. S., and Graf, W. H. (2004). "Scour depth and flow pattern of eroding plane jets." *Int. J. Sediment Res.*, 19(1), 15–27.

Powell, D. N., and Khan, A. A. (2011). "Sediment transport mechanics upstream of an orifice." *J. Visual.*, 14(4), 315–320.

Powell, D. N., and Khan, A. A. (2012). "Scour upstream of a circular orifice under constant head." *J. Hydraul. Res.*, 50(1), 28–34.

Prohaska, P. D., Khan, A. A., and Kaye, N. B. (2010a). "Investigation of detention pond outflow characteristics." *Water Manage.*, 163(3), 123–131.

Prohaska, P. D., Khan, A. A., and Kaye, N. B. (2010b). "Investigation of flow through orifices in riser pipes." *J. Irrig. Drain. Eng.*, 10.1061/(ASCE)IR.1943-4774.0000195, 340–347.

Raiford, J. P., and Khan, A. A. (2009). "Investigation of circular jets in shallow water." *J. Hydraul. Res.*, 47(5), 611–618.

Raiford, J. P., and Khan, A. A. (2013). "Turbulence schemes for modelling a submerged hydraulic jump." *Eng. Comput. Mech.*, 166(1), 40–51.

Rajaratnam, N., and Berry, B. (1977). "Erosion by circular turbulent wall jets." *J. Hydraul. Res.*, 15(3), 277–289.

Shammaa, Y., Zhu, D. Z., and Rajaratnam, N. (2005). "Flow upstream of orifices and sluice gates." *J. Hydraul. Eng.*, 10.1061/(ASCE)0733-9429(2005)131:2(127), 127–133.

Wu, S., and Rajaratnam, N. (1990). "Circular turbulent wall jets on rough boundaries." *J. Hydraul. Res.*, 28(5), 581–589.

Wu, W. (2008). *Computational river dynamics*, Taylor & Francis, Oxford, U.K.